# Exploiting Switching Transients for Broken Rotor Bar Detection in Inverter-Fed Induction Machines at All Operating Conditions

P. Nussbaumer, G. Stojicic, Th.M. Wolbank
Department of Energy Systems and Electrical Drives
Vienna University of Technology
Vienna, AUSTRIA

***Abstract*—In comparison to rotor bar fault detection for mains fed induction machines the detection in inverter-fed drives is especially challenging. The most important reasons are the disturbances introduced by the fast switching of the inverter. Moreover the fault indicator is influenced also by control dynamics and load changes. In addition most known fault detection technologies need a certain load level to ensure proper accuracy of the fault indicator. The proposed approach overcomes these drawbacks and allows accurate detection of rotor bar faults at all operating conditions. By applying special voltage pulse patterns using the inverter switching and identifying the currents reaction it is possible to calculate the machine's transient reactance. Due to rotor fault the distribution of the transient flux linkage is altered. This leads to a fault induced asymmetry in the spatial distribution of the transient reactance that can be used as a fault indicator. However, load condition influences the fault indicator. To eliminate this influence a compensation strategy using artificial neural networks is presented. Measurement results for healthy and faulty condition show the capbility of the novel rotor bar fault detection approach at different load conditions.**

***Keywords- Fault diagnosis; Harmonic analysis; Induction machines; Induction motor protection; Monitoring; Neural networks; Pulse width modulated inverters, Squirrel cage motors, Transient response***

## I. INTRODUCTION

Variable speed drives are widely used in industry. As higher reliability and fail safety become more and more important especially for security-relevant applications, the industry's demand for monitoring of inverter fed machines increases simultaneously. According to studies 5% to 10% of all drive breakdowns are caused by broken rotor bar defects [1]-[3]. The most common reason for this type of fault in mains fed induction machines is the additional stress during starting. As inverter operation offers the possibility to start the machine softly, one would think that broken rotor bars aren't an issue for this type of drives. However balancing of the motor is only possible at one speed, resulting in the fact that dynamic speed change causes additional stress on the rotor bars what may lead to rotor faults [4]. For medium and high power machines the copper bars in the rotor cage are typically brazed to the endring. However, aluminum and, to meet high efficiency requirements, copper die cast techniques are used in low power machines. According to studies the much higher coefficient of thermal expansion of aluminum and copper in comparison to the lamination steel in combination with repetitive thermal cycles due to high dynamic operation leads to high stress on the endring-bar connection. As a result a crack and finally a broken bar fault may develop over time.

Several different broken rotor bar detection methods have been proposed in literature [4]. The most common techniques are based on current signature analysis (CSA) [6]-[11]. A popular approach is to extract side bands in the spectrum of the stator current that can be used as fault indicator. In literature, a wide variety of different signal processing and harmonic analysis techniques can be found, such as Fourier transform [6], [7], wavelet approaches [8], [9], pattern recognition techniques [10] or neural networks [11], [12].

CSA-based rotor fault detection works well in mains fed operation under changing load conditions. However, these methods face difficulties when applied to inverter-fed machines due to increased noise level and changing operating frequency that usually limits fault detection to steady state and loaded operation.

To enable fault detection at changing stator frequency (10Hz/sec) Wiegner distribution is applied in [13]. Other fault detection techniques use fundamental-wave-models to extract a fault indicator. A comparison of the torque calculated by the stator equation and the one calculated by the rotor equation is proposed in [14]. Furthermore the virtual current of a fundamental-wave-model can be used to calculate a fault indicator, as described in [15]. The identification of the PWM's (pulse width modulation) low order harmonics ($6k\pm1$) to develop a rotor fault indicator is applied in [16], [17].

Due to the fact that in all of the aforementioned approaches the interaction of the defect bar with the machine's fundamental wave is exploited and the rotor cage is not "operating" at zero load if only considering the fundamental wave a certain minimum load level of around 30% to 40% has to be guaranteed.

Recently different approaches have been proposed that allow rotor fault detection at zero load and zero speed [18], [19] or almost zero speed [20]. These strategies can be used to monitor the machine whenever the drive is shut down.

The proposed method exploits the current response due to inverter switching. This current response is dominated by the

transient leakage inductance. A defect in the rotor cage will cause a distinct change in this transient inductance. However, the transient leakage inductance will also be influenced by the load level. This additional influence has to be determined in advance and will be eliminated using artificial neural network (ANN) techniques. The proposed approach offers the possibility to detect rotor bar faults at all operating conditions including zero load and speed with high accuracy.

## II. Asymmetry Detection by Exploiting Inverter Switching Transients

The following summarizes the measurement and signal processing steps needed to determine the fault indicator that is based on the evaluation of the transient leakage inductance. More details can be found in [20].

As stated before the detection method is based on evaluating the current change caused by a voltage step applied to the machine terminals. This voltage step is realized by changing the voltage source inverter's switching state. That is to say dc link voltage is applied to a machine phase for some 10µs, the current is measured at two different time instants using the built-in current sensors and the current change is calculated.

For an ideal symmetrical machine this reaction can be described by the well-known stator equation (1) in space vector representation.

$$\underline{v}_S = r_S \cdot \underline{i}_S + l_{l,t} \cdot \frac{d\underline{i}_S}{d\tau} + \frac{d\underline{\lambda}_R}{d\tau} \tag{1}$$

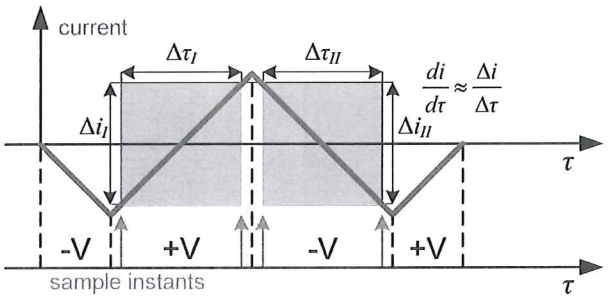


Fig. 1. Voltage switching pattern and current reaction for one phase

The dominant voltage drops during these short voltage steps are the machine's back EMF (electromotive force) $d\underline{\lambda}_R/d\tau$ (time derivative of rotor flux $\underline{\lambda}_R$) and the transient leakage inductance $l_{l,t}$ (differs from fundamental wave inductance $l_l$) times the time derivative of the stator current $\underline{i}_S$. $\underline{v}_S$ represents the machine's stator voltage phasor. To identify the transient leakage inductance the back EMF's influence has to be eliminated because of its speed dependency. This is done by applying two subsequent voltage pulses (switching states, denoted with indexes *I* and *II*). During the short time interval of some ten µs the direction and magnitude of the machine's back EMF will only change negligible and subtraction of the two step responses will eliminate this influence. By applying a special switching pattern, as shown in Fig. 1, to keep the fundamental wave point of operation unchanged during the voltage pulses the voltage drop caused by the stator resistance $r_S$ is eliminated as well. This leads to the fact that the stator resistance's significant temperature dependence doesn't influence the measurement result. With the special switching pattern applied to the machine terminals the back EMF ($d\underline{\lambda}_{R,I}/d\tau \approx d\underline{\lambda}_{R,II}/d\tau$) and the stator current ($\underline{i}_{S,I} = \underline{i}_{S,II}$) during the two switching states *I* and *II* can be assumed constant. The subtraction results in the equation illustrated in (2).

$$\underline{v}_{S,I-II} = \underline{v}_{S,I} - \underline{v}_{S,II} = l_{l,t}\left(\frac{d\underline{i}_{S,I}}{d\tau} - \frac{d\underline{i}_{S,II}}{d\tau}\right) \tag{2}$$

Considering a machine under fault condition the transient leakage inductance is no longer a scalar, it is a complex value $\underline{l}_{l,t}$ combining a symmetrical $l_{offset}$ and complex portion $\underline{l}_{mod}$ representing the fault induced asymmetry in magnitude $l_{mod}$ and spatial direction $\delta$. This complex portion points in the direction of maximum inductance within each pole in case of rotor faultpair. That is to say if the rotor is turned over one mechanical revolution the influence of the broken bar on the transient leakage induction will be repeated for every pole of the stator winding. This circumstance is expressed for a two-pole machine in (3) by choosing the angle of $\underline{l}_{mod}$ to $2\delta$. Inserting (3) in (2) and inverting the resulting equation to reduce the necessary mathematical operations leads to (4). The complex conjugate of the stator voltage phasor is denoted $\underline{v}_S^*$.

$$\underline{l}_{l,t} = l_{offset} + \underline{l}_{\mathrm{mod}}, \quad \underline{l}_{\mathrm{mod}} = l_{\mathrm{mod}} \cdot e^{j2\delta} \tag{3}$$

$$\frac{d\underline{i}_{S,I-II}}{d\tau} = y_{offset} \cdot \underline{v}_{S,I-II} + \underline{y}_{mod} \cdot \underline{v}^*_{S,I-II}, \quad \frac{d\underline{i}_{S,I-II}}{d\tau} = \underline{y}_{I-II} \cdot \underline{v}_{S,I-II} \tag{4}$$

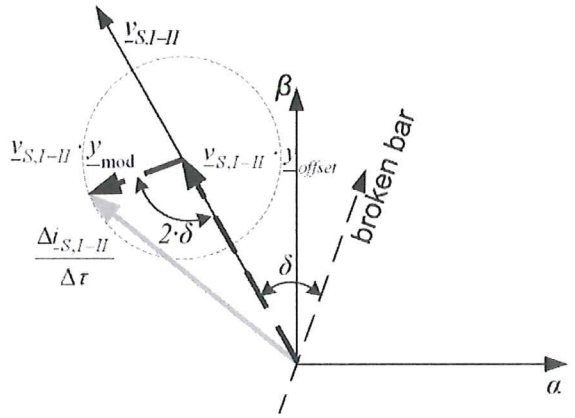


Fig. 2. Resulting current change vector (gray) after signal processing for switching pattern applied to phase V ($v_{S,I}$=V+ and $v_{S,II}$=V-); asymmetry in direction $\delta$=70° denoted 'broken bar'.

The relations of the statements above are illustrated in the stator-fixed frame of reference in Fig. 2 for application of the switching pattern in phase V (+V,-V, as shown in Fig. 1). The time derivative of the stator current $d\underline{i}_S/d\tau$ is approximated by

its difference $\Delta \underline{i}_S/\Delta\tau$ leading to the following equation, that describes the inverse transient leakage induction $\underline{y}_{I\text{-}II}$

$$\underline{y}_{I-II} = \frac{\frac{\Delta \underline{i}_{S,I-II}}{\Delta\tau}}{\underline{v}_{S,I-II}} \tag{5}$$

There are several ways to eliminate the share of the transient inductance's symmetrical part $y_{offset}$. The one used in the present investigation is to change the applied voltage excitation to all phase directions and calculating the resulting phasor $\underline{c}$ that contains the whole information about the machine's asymmetry (denoted asymmetry phasor in the following). The symmetrical part then leads to a zero sequence component and hence is eliminated. The calculation of the asymmetry phasor is shown in (6). $\underline{y}_{I\text{-}II,U}$, $\underline{y}_{I\text{-}II,V}$ and $\underline{y}_{I\text{-}II,W}$ indicate the transient leakage inductances calculated during the corresponding voltage switching pattern for each phase U, V and W.

$$\underline{c} = \frac{2}{3} \cdot \left( \underline{y}_{I-II,U} + \underline{y}_{I-II,V} \cdot e^{j\frac{2\pi}{3}} + \underline{y}_{I-II,W} e^{j\frac{4\pi}{3}} \right) \tag{6}$$

The fault induced asymmetry however, is not the only asymmetry present in a machine. Every machine, if faultless or not, has some inherent asymmetries for example caused by the machine's mechanical geometry (e.g. rotor/stator slotting) or spatial saturation. In the asymmetry phasor all these asymmetries are superposed. The modulation period due to spatial saturation asymmetry strongly depends on the machine's load and flux level and may superpose with the modulation period caused by broken bar faults. To realize accurate rotor fault detection this dependency has to be identified in advance and eliminated from the asymmetry phasor signal.

In the proposed approach this elimination is done by using ANN techniques.

## III. Artifical Neural Networks

The saturation induced asymmetry is visible as a second harmonic with respect to the fundamental wave in the asymmetry phasor's frequency spectrum.

The ANN used to compensate the portion caused by saturation in the asymmetry phasor is of multi layer perceptron (MLP) type. A comparison of different ANN types, like MLP, functional link neural networks (FNL) and time delay neural networks can be found in [21]. As was shown, the MLP type is the best suited one for this type of application.

The applied MLP-ANN consists of three layers: the input layer (two neurons), the hidden layer (12 neurons) and the output layer (two neurons). The load current and an offset of constant one are the inputs to the ANN. The Output provides magnitude and angle of the asymmetry phasor's harmonic corresponding to the saturation asymmetry. The structure of a typical multi layer perceptron neural network is shown in the following Fig. 3.

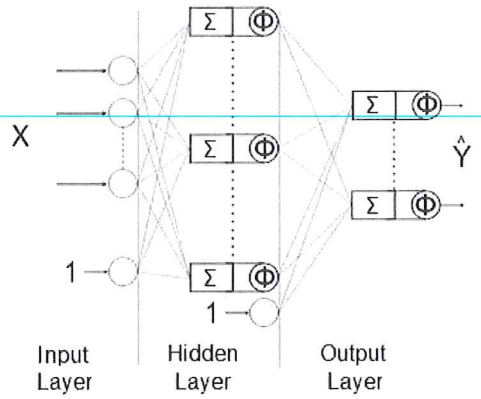


Fig. 3. Neural network structure

During the training phase the asymmetry phasor is calculated and collected for different flux angles. In a second step the asymmetry phasor's fast Fourier transform (FFT) is determined. For the identification of the saturation induced harmonic the Fourier spectrum is always generated with respect to the fundamental wave. In this case the saturation induced harmonic always results in a 2nd harmonic independent of the load condition, what makes the identification of the saturation induced portion in the asymmetry phasor very easy. The 2nd harmonic's magnitude and orientation are collected for different load conditions and are used as the reference values in the training phase. The training is done offline and the gained input and output weights are then used for the online phase of the monitoring procedure. The trained ANN is then capable of interpolating between the data that had been collected during the training phase and all other operating conditions with high accuracy. Different methods for ANN-learning have been developed in the last decades. These methods can be separated basically into two groups – supervised or unsupervised. The chosen technique in the proposed approach is the most popular of the supervised learning methods, namely the back propagation network (BPN) [22]. It combines the advantages of high learning accuracy and high recall speed.

## IV. Saturation Compensation using ANN Techniques

For the calculation of the fault indicator the asymmetry phasor over one mechanical period is taken into account. Therefore a rotor fault always appears as a harmonic equaling the machine's number of poles in the spectrum of the asymmetry phasor what leads to simple identification of the fault indicator. However, the order of the saturation induced harmonic then depends on the machine's slip, the magnitude on the load condition. Depending on the operating condition the fault and saturation induced harmonic components in the asymmetry phasor signal may overlap. For no-load-operation the rotor fault and the saturation harmonic result in a harmonic equaling the number of poles in the Fourier spectrum of the asymmetries phasor with respect to one mechanical revolution as the synchronous equals the rotor rotation speed (zero slip). For loaded operation the slip frequency is unequal to zero. Therefore, in motor drive operation after a mechanical

revolution the flux took more than one revolution (times the number of pole pairs). The order of the saturation induced harmonic with respect to one mechanical revolution doesn't equal exactly the number of poles anymore, but still adds a considerable portion to the fault induced harmonic. Furthermore in high dynamic operation the load condition could change during the measurement procedure. In that case the saturation induced portion in the asymmetry phasor for different rotor positions may vary. By directly compensating the saturation induced portion in the asymmetry phasor using an ANN it is possible to ensure accurate fault detection independent of the induction machine's operating state including zero load.

As stated before the ANN delivers the magnitude $c_{sat}$ and angle $\theta_{sat}$ of the saturation induced harmonic in the Fourier spectrum of the asymmetry phasor signal over one fundamental wave period for the current operating state. The magnitude of this harmonic $c_{sat}$ equals the absolute value of the saturation induced portion in the asymmetry phasor, whereas the argument $\theta_{sat}$ equals the angle between the stator current phasor and the saturation induced portion of the asymmetry phasor in the stator-fixed frame of reference. If this information is combined with the current phase angle $\gamma_{el}$ of the fundamental wave the saturation induced portion $\underline{c}_{sat}$ of the current asymmetry phasor $\underline{c}$ can be calculated and hence eliminated as shown in (7). The saturation compensated asymmetry phasor $\underline{c}_{comp}$ remains. In (7) $p$ represents the machine's number of pole-pairs.

$$\underline{c}_{sat} = c_{sat} \cdot e^{j(2 \cdot p \cdot \gamma_{el} + \theta_{sat})} \qquad \underline{c}_{comp} = \underline{c} - \underline{c}_{sat} \tag{7}$$

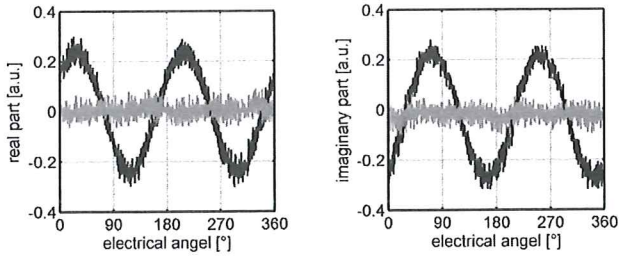


Fig. 4. Real (left) and imaginary part (right) of asymmetry phasor's trajectory over one fundamental wave period for a faultless machine at rated flux and 40% load (gray: saturation compensated, black: uncompensated)

Real- and imaginary-part of the asymmetry phasor's trajectory over a fundamental wave period are shown in Fig. 4. The black trace shows the uncompensated real and imaginary part, the gray the compensated ones at rated flux and 40% load for a faultless machine. As the investigated machine has 28 rotor slots this would result in a positive or negative 28$^{th}$ harmonic in the asymmetry phasor's frequency-spectrum with respect to one mechanical revolution depending on the mechanical construction. In dependency on the induction machine's operating condition, that is to say the machine's speed and load, the order of this so-called slotting harmonic in the asymmetry phasor's Fourier-spectrum with respect to the fundamental wave period varies. The reason for this is that, for different slip, the number of passed rotor slots during one revolution of the flux is varying. At no load operation the number of passed rotor slots equals the total number of slots $n_r$ resulting in a $n_r^{th}$ harmonic in the asymmetry phasor's Fourier spectrum over one mechanical revolution as well as in the asymmetry phasor's Fourier spectrum with respect to the fundamental wave. For loaded motor operation the order of the rotor slotting harmonic is lower than $n_r$ if the Fourier-spectrum is calculated with respect to the fundamental wave and equal to $n_r$ with respect to one mechanical revolution. The slotting harmonic is already extracted in Fig. 4 and Fig. 5.

As can be seen in Fig. 4 the disturbing influence due to saturation could be clearly reduced due to the application of the proposed ANN-based compensation algorithm.

The spectrum of the asymmetry phasor over one fundamental wave period is shown in Fig. 5. The left figure shows the spectrum before and the right after compensation at rated flux and 40% load for a faultless induction machine. The disturbing influence of the saturation could be clearly reduced from 0.242 to nearly zero.

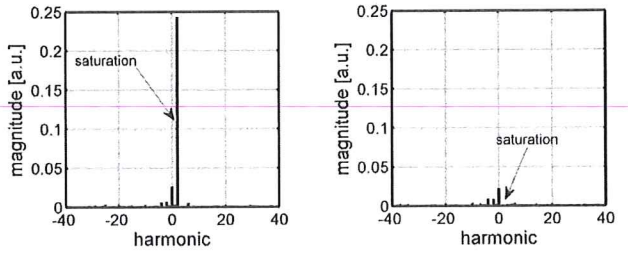


Fig. 5. Uncompensated (left) and compensated (right) FFT spectrum of asymmetry phasor over a fundamental wave period for a faultless machine at rated flux and 40% load (artificial unit a.u.)

After the compensation of the saturation induced portion in the asymmetry phasor signal the main operating dependent influence that may disturb the fault indicator has been eliminated. Therefore high sensitive and accurate fault detection can be guaranteed.

## V. Calculation of the Fault Indicator

To better understand the proposed rotor fault detection procedure Fig. 6 shows a block diagram describing the signal path from excitation to identification of the fault indicator.

The first step is to excite the machine with the described voltage pattern (see Fig. 1). With linear combination of the approximated current derivative space vector $\Delta \underline{i}_S/\Delta\tau$ the asymmetry phasor can be calculated for the current rotor position. As mentioned before this asymmetry phasor contains a load dependent saturation induced component that lowers the accuracy of the fault detection. This dependency is eliminated with the help of ANN techniques as described above. The saturation compensated asymmetry phasor is stored in a buffer. After one mechanical revolution the buffer is filled up with asymmetry phasor for different rotor positions. A rotor fault results in the Fourier spectrum of all collected asymmetry phasor over one mechanical revolution as a harmonic equaling the induction machine's number of poles. This harmonic can be extracted from the frequency spectrum and represents the fault

indicator. The fault indicator's magnitude correlates with the fault severity, the phase angle with the fault position.

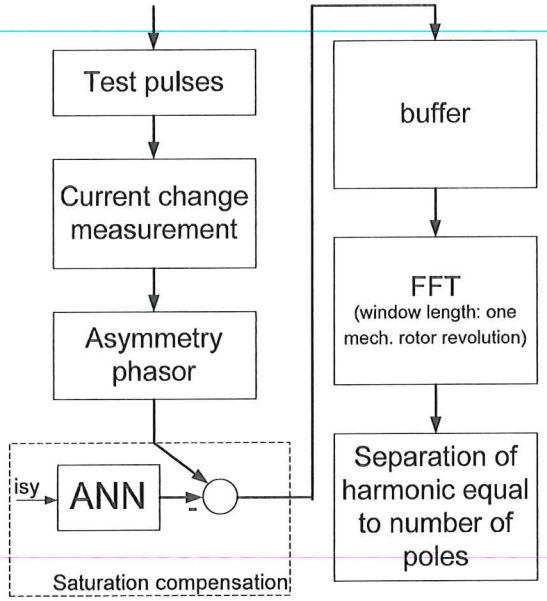


Fig. 6. Block diagram of pulse excitation, measurement, saturation compensation and signal processing structure

## VI. Experimental Results

Measurements were performed on a 5kW, 2-poles, inverter-fed induction machine with a specially manufactured 28 slot rotor that allows removing single rotor bars. The measurement procedure is not limited to small scale machines however. Measurements were carried out with one bar removed and one of the 28 copper bars replaced with one brass bar. With this last measurement it can be verified that the proposed method is capable to detect not only an already broken copper bar but also a resistance increase in a single bar. That is to say a developing broken rotor bar fault. The replacement of a single copper bar with a brass one results in a relative resistance increase with a factor of 3,74 in this single bar.

To identify the fault condition of a machine the asymmetry phasor is collected over one whole rotor revolution, as stated above. The influence of a broken bar is repeated for every pole. Therefore an increased 2nd harmonic in the asymmetry phasor's frequency spectrum with respect to one mechanical revolution for a 2-poles machine, as used in the present investigation, indicates a fault. When compensating the saturation asymmetry from the asymmetry phasor the increase is independent of the operating state for constant fault condition.

Fig. 7 shows the frequency spectrum (saturation compensated) of the asymmetry phasor over one mechanical revolution for faultless (left) and defective condition (right; one broken bar) at rated flux and 40% load. The very distinct increase in magnitude of the asymmetry phasor's 2nd harmonic (from $3.86 \cdot 10^{-3}$ to $96.8 \cdot 10^{-3}$) by a factor of ~25 in the right spectrum indicates the broken bar rotor fault.

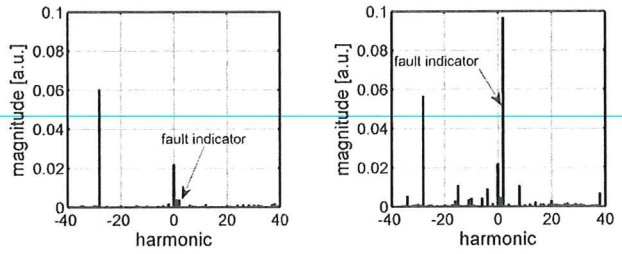


Fig. 7. FFT spectrum of asymmetry phasor over one mechanical revolution for a faultless (left) and defective machine with one broken bar (right) at rated flux and 40% load; saturation compensated (artificial units a.u.)

The very distinct change in the case of only one broken bar leads to the assumption that the proposed monitoring procedure might be sensitive enough to even detect a developing rotor fault. Therefore further measurements with one copper rotor bar replaced by a brass bar were carried out. For this fault condition an increase of the fault indicator to $11.4 \cdot 10^{-3}$ could be determined. This is still clearly distinguishable from the healthy condition. The frequency spectrum over one mechanical revolution for the healthy rotor (left) and the machine with developing rotor fault (right) is shown in Fig. 8. For both measurement results the saturation was compensated by application of the proposed technique.

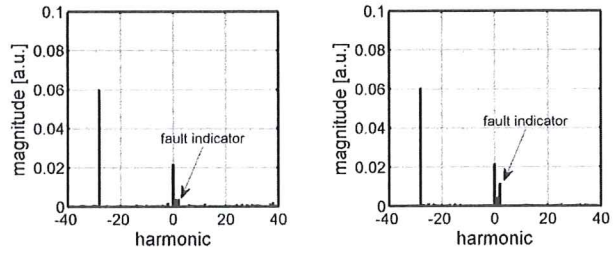


Fig. 8. FFT spectrum of asymmetry phasor over one mechanical revolution for a faultless (left) and a machine with developing rotor fault (right; increased resistance of 374 % in a single bar) at rated flux and 40% load; saturation compensated (a.u. … artificial unit)

To proof that the proposed method is able to detect a rotor fault independent of the operating condition several measurements at various load conditions were performed. As the presented ANN-based saturation compensation technique eliminates all operation-point-dependent disturbances of the fault indicator, the magnitude of the fault indicator has to be nearly constant for all measurements at different load conditions. This is shown in Fig. 9 for both investigated fault conditions.

Due to the fact that the fault indicator remains constant for different load conditions it can be verified that the saturation induced portion in the asymmetry phasor can be accurately compensated. Therefore reliable fault detection can be ensured even under high dynamic load changes during the measurement procedure.

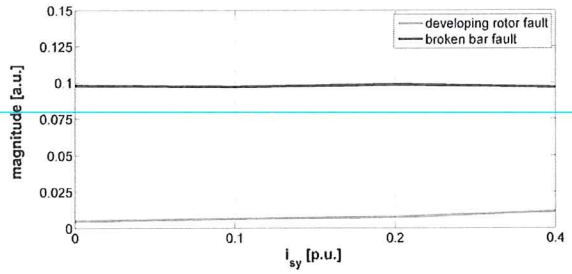


Fig. 9. Fault indicator at different load conditions from zero to 40% load at rated flux for broken bar fault (black) and developing rotor fault (gray; one single copper bar replaced by brass)

## VII. CONCLUSION

The proposed procedure uses the induction machine's transient leakage inductance to detect a rotor fault. By compensating the flux and load dependent components in the observed asymmetry phasor with ANN techniques it is possible to obtain a fault indicator independent of the drive's operating condition.

Measurement results show that the fault indicator's dependence on the operating point is eliminated reliably. It is verified that the proposed method is able to detect rotor faults at different operating conditions with high sensitivity and accuracy. Due to the fact that the fault indicator is independent of the machine's operating point even dynamic load changes during the measurement procedure don't influence the measurement results. Two different fault conditions – a broken bar fault and a developing broken bar fault – are investigated. In both cases the fault indicator is clearly distinguishable from the healthy condition and accurate detection and separation of different fault conditions can be guaranteed. The proposed approach allows continuous online monitoring of the drive independent of the operating condition.

## REFERENCES


[1] A. H. Bonnet and C. Yung, "Increased efficiency versus increased reliability," *IEEE Industry Applications Magazine,* vol.14, no.1, pp.29-36, 2008.

[2] IEEE Committee Report, "Report of large motor reliability survey of industrial and commercial installation, Part I," *IEEE Transactions on Industry Applications*, vol.21, no.4, pp.853–864, Jul./Aug. 1985.

[3] IEEE Committee Report, "Report of large motor reliability survey of industrial and commercial installation, Part II," *IEEE Transactions on Industry Applications*, vol.21, no.4, pp.865–872, Jul./Aug. 1985.

[4] M. Hodowanec and W. R. Finley, "Copper versus Aluminum - Which Construction is Best?," *IEEE Industry Applications Magazine,* vol.8, no.4, pp. 14-25, 2002.

[5] A. Bellini, F. Filippetti, C. Tassoni and G. Capolino, "Advances in Diagnostic Techniques for Induction Machines," *IEEE Transactions on Industrial Electronics,* vol.55, no.12, pp.4109-4126, 2008.

[6] W. Le Roux, R. G. Harley and T. G. Habetler, "Detecting Rotor Faults in Low Power Permanent Magnet Synchronous Machines," *IEEE Transactions on Power Electronics,* vol.22, no.1, pp.322-328, 2007.

[7] A. Khezzar, M. Y. Kaikaa, M. E. K. Oumaamar, M. Boucherma, and H. Razik, "On the use of SLot harmonics as a potential indicator of rotor bar breakage in the induction machine," *IEEE Trans. Ind. Electron.*, vol. 56, no. 11, pp. 4592–4605, 2009.

[8] S.H. Kia, H. Henao and G. Capolino, "Diagnosis of Broken Bar Fault in Induction Machines Using Discrete Wavelet Transform without Slip Estimation," *IEEE Transactions on Industry Applications,* vol.45, no.4, pp.1395-1404, 2009.

[9] M. Riera-Guasp, J. A. Antonino-Daviu, M. Pineda-Sanchez, R. Puche-Panadero and J. Perez-Cruz, "A General Approach for the Transient Detection of Slip-Dependent Fault Components Based on the Discrete Wavelet Transform," *IEEE Transactions on Industrial Electronics,* vol.55, no.12, pp.4167-4180, 2008.

[10] M. Haji and H. A. Toliyat, "Pattern Recognition - a Technique for Induction Machines Rotor Fault Detection eccentricity and Broken Bar Fault," *Proceedings of Industry Applications Annual Conference IAS,* vol.3, pp.1572-1578, 2001

[11] B. Ayhan, M.-Y. Chow and M.-H. Song, "Multiple Discriminant Analysis and Neural-Network-Based Monolith and Partition Fault-Detection Schemes for Broken Rotor Bar in Induction Motors," *IEEE Transactions on Industrial Electronics,* vol.53, no.4, pp.1298-1308, 2006.

[12] F. Filippetti, G. Franceschini and C. Tassoni, "Neural networks aided on-line diagnostics of induction motor rotor faults," *IEEE Transactions on Industry Applications,* vol.31, no.4, pp.892-899, 1995.

[13] M. Blödt, D. Bonacci, J. Regnier, M. Chabert and J. Faucher, "On-Line Monitoring of Mechanical Faults in Variable-Speed Induction Motor Drives Using the Wigner Distribution," *IEEE Transactions on Industrial Electronics,* pp.522-531, 2008.

[14] C. Kral, F. Pirker, G. Pascoli, H. Kapeller, "Robust Rotor Fault Detection by Means of the Vienna Monitoring Method and a Parameter Tracking Technique," *IEEE Transactions on Industrial Electronics,* vol.55, no.12, pp. 4229-4237, 2008.

[15] S. M. Cruz, A. Stefani, F. Filippetti and A. J. Marques Cardoso, "A New Model-Based Technique for the Diagnosis of Rotor Faults in RFOC Induction Motor Drives," *IEEE Transactions on Industrial Electronics,* vol.55, no.12, pp.4218-4228, 2008.

[16] B. Akin, U. Orguner, H. Toliyat, and M. Rayner, "Low order PWM inverter harmonics contributions to the inverter-fed induction machine fault diagnosis," *IEEE Trans. Ind. Electron.*, vol. 55, no. 2, pp. 610–619, Feb. 2008.

[17] C. Bruzzese, "Analysis and application of particular current signatures (symptoms) for cage monitoring in nonsinusoidally fed motors with high rejection to drive load, inertia, and frequency variations," IEEE Trans. Ind. Electron., vol. 55, no. 12, pp. 4137–4155, Dec. 2008.

[18] B. Kim, K. Lee, J. Yang, S. B. Lee, E. Wiedenbrug and M. Shah, "Automated detection of rotor faults for inverter-fed induction machines under standstill conditions," *IEEE Energy Conversion Congress and Exposition,* pp.2277-2284, 2009.

[19] C. Concari, G. Franceschini and C. Tassoni, "Self-commissioning procedures to detect parameters in healthy and faulty induction drives," *Proceedings of IEEE International Symposium on Diagnostics for Electric Machines, Power Electronics and Drives, SDEMPED,* pp.1-6, 2009.

[20] T.M. Wolbank, P. Nussbaumer, H. Chen, and P. Macheiner, "Non-invasive detection of rotor cage faults in inverter fed induction machines at no load and low speed", *Proceedings of IEEE International Symposium on Diagnostics for Electric Machines, Power Electronics and Drives, SDEMPED,* pp.1-7, 2009.

[21] T.M. Wolbank, M.A. Vogelsberger, R. Stumberger, S. Mohagheghi, T.G. Habetler, R.G. Harley, "Comparison of Neural Network Types and Learning Methods for Self Commissioning of Speed Sensorless Controlled Induction Machines," *IEEE Power Electronics Specialists Conference, 2007. PESC 2007,* pp.1955-1960, 2007.

[22] S.S.Haykin, "Neural Networks: A Comprehensive Foundation," Prentice Hall, 2nd Edition, ISBN 0- 1327-3350-1, 1998.